NeuroImage: Clinical 20 (2018) 1018–1025

Contents lists available at ScienceDirect

NeuroImage: Clinical

journal homepage: www.elsevier.com/locate/ynicl

Atrophy, metabolism and cognition in the posterior cortical atrophy spectrum based on Alzheimer's disease cerebrospinal fluid biomarkers

Maxime Montembeault[a,b,c,d], Simona M. Brambati[c,d], Foudil Lamari[e], Agnès Michon[f], Dalila Samri[f], Stéphane Epelbaum[f], Lucette Lacomblez[g,h,i], Stéphane Lehéricy[b,j], Marie-Odile Habert[g,k], Bruno Dubois[a,b,f], Aurélie Kas[g,k,*,1], Raffaella Migliaccio[a,b,f,*,1]

[a] FrontLab, Institut du Cerveau et de la Moelle épinière (ICM), 75013 Paris, France
[b] INSERM U 1127, CNRS UMR 7225, Sorbonne Universités, Université Pierre et Marie Curie-Paris 6, UMR S1127, Institut du Cerveau et de la Moelle épinière (ICM), Pitié-Salpêtrière hospital, 75013 Paris, France
[c] Centre de recherche de l'Institut Universitaire de Gériatrie de Montréal, H3W 1W6 Montréal, QC, Canada
[d] Department of Psychology, University of Montreal, H2V 2S9 Montréal, QC, Canada
[e] Department of Metabolic biochemistry, Pitié-Salpêtrière hospital, 75013 Paris, France
[f] Department of Nervous system diseases, Institut de la mémoire et de la maladie d'Alzheimer (IM2A), Neurology, Pitié-Salpêtrière hospital, 75013 Paris, France
[g] LIB, Inserm U1146, Université Pierre et Marie Curie, Paris 6, 75006 Paris, France
[h] Department of Nervous system diseases, CIC-CET, Pitié-Salpêtrière hospital, 75013 Paris, France
[i] Pharmacology service, Pitié-Salpêtrière hospital, 75013 Paris, France
[j] Centre de Neuro-imagerie de Recherche (CENIR) de l'Institut du Cerveau et de la Moelle Epiniere (ICM), Hôpital de la Pitié-Salpêtrière, 75013 Paris, France
[k] Department of Nuclear Medicine, Pitié-Salpêtrière hospital, 75013 Paris, France

ARTICLE INFO

Keywords:
Posterior cortical atrophy
Alzheimer's disease
Cerebrospinal fluid
Biomarkers
Gray matter atrophy
Brain metabolism
Neuropsychology
Atypical dementia
^{18}F-FDG PET
Voxel-based morphometry

ABSTRACT

Introduction: *In vivo* clinical, anatomical and metabolic differences between posterior cortical atrophy (PCA) patients presenting with different Alzheimer's disease (AD) cerebrospinal fluid (CSF) biomarkers profiles are still unknown.

Methods: Twenty-seven PCA patients underwent CSF examination and were classified as 1) PCA with a typical CSF AD profile (PCA-tAD; abnormal amyloid and T-tau/P-tau biomarkers, n = 13); 2) PCA with an atypical AD CSF profile (PCA-aAD; abnormal amyloid biomarker only, n = 9); and 3) PCA not associated with AD (PCA-nonAD; normal biomarkers, n = 5). All patients underwent clinical and cognitive assessment, structural MRI, and a subset of them underwent brain ^{18}F-FDG PET.

Results: All patients' groups showed a common pattern of posterior GM atrophy and hypometabolism typical of PCA, as well as equivalent demographics and clinical/cognitive profiles. PCA-tAD patients showed a group-specific pattern of hypometabolism in the left fusiform gyrus and inferior temporal gyrus. PCA-aAD did not present a group-specific atrophy pattern. Finally, group-specific gray matter atrophy in the right dorsolateral prefrontal cortex, left caudate nucleus and right medial temporal regions and hypometabolism in the right supplementary motor area and paracentral lobule were observed in PCA-nonAD patients.

Conclusion: Our findings suggest that both PCA-tAD and PCA-aAD patients are on the AD continuum, in agreement with the recently suggested A/T/N model. Furthermore, in PCA, the underlying pathology has an impact at least on the anatomo-functional presentation. Brain damage observed in PCA-tAD and PCA-aAD was mostly consistent with the well-described presentation of the disease, although it was more widespread in PCA-tAD group, especially in the left temporal lobe. Additional fronto-temporal (especially dorsolateral prefrontal)

Abbreviations: $A\beta_{1-42}$, amyloid beta1–42; AD, Alzheimer's disease; CBD, corticobasal degeneration; CSF, cerebrospinal fluid; CTRL, healthy control subjects; DLB, dementia with Lewy bodies; ^{18}F-FDG, 2-Deoxy-2-[F-18]fluoro-D-glucose; GM, gray matter; MMSE, Mini-Mental State Exam; MRI, magnetic resonance imaging; PCA, Posterior cortical atrophy; PCA-tAD, PCA patients with typical CSF AD profile; PCA-aAD, PCA patients with an atypical CSF AD profile; PCA-nonAD, PCA patients who did not present any element of the CSF AD profile; PET, Positron emission tomography; P-tau, phosphorylated tau; SPECT, single-photon emission computed tomography; T-tau, total tau; VBM, voxel-based morphometry

* Corresponding author at: FrontLab, INSERM U 1127, CNRS UMR 7225, Sorbonne Universités, Université Pierre et Marie Curie-Paris 6, UMR S1127, Institut du Cerveau et de la Moelle épinière (ICM), Pitié-Salpêtrière Hospital, 75013 Paris, France.
E-mail address: lara.migliaccio@gmail.com (R. Migliaccio).
[1] These authors equally contributed to the article.

https://doi.org/10.1016/j.nicl.2018.10.010
Received 2 June 2018; Received in revised form 25 September 2018; Accepted 8 October 2018
Available online 10 October 2018

damage seems to be a clue to underlying non-AD pathology in PCA, which warrants the need for longitudinal follow-ups to investigate frontal symptoms in these patients.

1. Introduction

Posterior cortical atrophy (PCA) is a rare neurodegenerative syndrome mainly characterized by progressive high-level visual and visuomotor impairments, in the absence of ophthalmologic impairment (Benson et al., 1988; Migliaccio et al., 2012a). The most frequent clinical manifestations include elements of Balint's and Gerstmann's syndromes, visual agnosia, alexia, apraxia and environmental disorientation (McMonagle et al., 2006). PCA is associated with bilateral parietal, occipital and posterior temporal gray matter (GM) atrophy (Whitwell et al., 2007) and hypometabolism (Kas et al., 2011), and it has been shown that brain damage remains posterior even in the late stages of the disease (Kas et al., 2011).

Previous clinico-biological (Beaufils et al., 2013; Beaufils et al., 2014; Coppi et al., 2014; de Souza et al., 2011a; de Souza et al., 2011b; Seguin et al., 2011) and clinico-pathologic (Renner et al., 2004; Tang-Wai et al., 2004) series have shown that the most frequent neuropathological substrate of PCA is Alzheimer's disease (AD) pathology. For this reason, PCA is considered an atypical variant of AD, in patients with early age at onset (Benson et al., 1988; Migliaccio et al., 2009; Panegyres et al., 2017). The AD cerebrospinal fluid (CSF) biomarkers' profile is characterized by high levels of total tau (T-tau) and phosphorylated tau at threonine 181 (P-tau), combined with a reduction of amyloid beta$_{1–42}$ (A$\beta_{1–42}$), and represents the most sensitive and specific tool to diagnose AD pathology *in vivo* (de Souza et al., 2011b; Dubois et al., 2014). However, some PCA patients can present an atypical AD CSF profile (i.e. only decreased A$\beta_{1–42}$ or only increased tau) (Beaufils et al., 2013; Beaufils et al., 2014; Coppi et al., 2014; Seguin et al., 2011) or a non-AD CSF profile (Renner et al., 2004; Seguin et al., 2011; Tang-Wai et al., 2004). This is in the vein of the suggested A/T/N model of AD (Jack Jr. et al., 2018; Jack Jr. et al., 2016), a descriptive system for categorizing multidomain biomarker findings at the individual person level. This model considers three elements: the value of β-amyloid biomarker (amyloid PET or CSF A$\beta_{1–42}$, A); the value of tau biomarker (CSF P-tau, or tau PET, T); and biomarkers of neurodegeneration or neuronal injury ([18F]-fluorodeoxyglucose–PET, structural MRI, or CSF T-tau, **N**). With the movement of the amnestic AD research field towards the A/T/N model, it is essential for clinically atypical AD patients (such as PCA patients) to also be characterized in the perspective of this model.

In this study, we aimed to investigate GM density, brain metabolism and clinical/cognitive profiles in a large sample of 27 PCA patients according to their AD CSF biomarkers profiles. Despite the growing number of observations, *in vivo* clinico-anatomical differences between PCA patients presenting with these different CSF biomarkers profiles are still unknown. We hypothesized that PCA patients with different AD CSF profiles have different patterns of brain damage and clinical/cognitive presentation.

2. Material and methods

2.1. Subjects

Twenty-seven PCA patients, 30 age-matched healthy subjects with available magnetic resonance imaging (MRI) scan and 17 age-matched healthy subjects with available positron emission tomography (PET) scan (CTRL, without history of neurological or psychiatric disease) participated in this study. Clinical and cognitive data were acquired at the Centre National de Référence “Démences Rares”, located at the “Institut de la mémoire et de la maladie d'Alzheimer” (IM2A), in the Pitié-Salpêtrière Hospital, Paris. Clinical diagnosis was based on a multi-disciplinary evaluation including clinical history and neurological examination, caregiver interview, and neuropsychological battery. Neurological assessment and diagnosis were performed by trained clinicians (R.M., L.L., A.M., S.E. and B.D.) with expertise in the field of dementia. Medical records of patients clinically diagnosed with PCA were reviewed by a neurologist (R.M.) and a neuropsychologist (M.M.) to ensure they met PCA diagnostic criteria. Diagnosis of PCA was made based on: 1) presentation with progressive visual or visuospatial impairment in the absence of ophthalmologic impairment; 2) evidence of complex visual disorder on examination: elements of Balint's and Gerstmann's syndrome, visual agnosia, alexia, apraxia, or environmental disorientation; 3) proportionately less memory loss (Alladi et al., 2007; McMonagle et al., 2006). To meet criteria, patients were required to present with early complaints of visual and visuospatial impairment in the absence of major memory complaints. Exclusion criteria for this study included history of other neurological or psychiatric diseases, ophthalmologic disease, extrapyramidal symptoms or signs, hallucinations, cognitive fluctuations, left-handedness, rapidly evolving dementia syndromes, or substantial MRI T2 white matter hyperintensities in the occipito-parietal regions.

PCA patients were then divided in groups based on AD CSF biomarkers. The AD CSF signature usually combines low A$\beta_{1–42}$ and high T-tau or P-tau concentrations (Dubois et al., 2014). In this study, A$\beta_{1–42}$, T-tau and P-tau were measured for each patient [for procedure see (Teichmann et al., 2013)]. Two ratios obtained in a previous study from our department were used as the main inclusion criterion to determine if a patient presented the AD CSF signature, namely a T-tau/A$\beta_{1–42}$ cut-off of < 1.23 pg/ml and a P-tau/A$\beta_{1–42}$ cut-off of < 0.211 pg/ml (de Souza et al., 2011b). These ratios have respective sensitivities of 95% and 91.7%, and respective specificities of 84.8% and 89.1% in distinguishing AD from other neurodegenerative dementias involving pathological processes distinct from AD. In addition to ratios, individual biomarkers levels were also considered for A$\beta_{1–42}$ (cut-off normal $>$ 500 pg/ml), T-tau (normal < 450 pg/ml) and P-tau (normal < 60 pg/ml) (Baldacci et al., 2017).

Patients with typical CSF AD profile (PCA-tAD) were defined as follow: at least one pathological ratio, and low A$\beta_{1–42}$ combined with higher T-tau and/or P-tau. Patients presenting with an isolated reduction of A$\beta_{1–42}$ were defined as having an atypical CSF AD profile (PCA-aAD) (Seguin et al., 2011), in agreement with the fact that isolated A$\beta_{1–42}$ reduction may indicate an amyloidogenic process (McKhann et al., 2011). Patients who did not present any element of the CSF AD profile were classified as PCA-nonAD. The study was approved by the local committee on human research. All subjects provided written informed consent before participating.

2.2. Clinical/cognitive assessment

All patients underwent a neuropsychological screening battery including a global cognitive assessment with the Mini-Mental State Examination (MMSE) (Folstein et al., 1975) as well as an assessment of “frontal” brain functions with the Frontal Assessment Battery (FAB) (Dubois et al., 2000), backwards digit and visual span (Wechsler, 1981), and word generation tasks for category and letter fluency (Kremin et al., 1999). Patients' scores on these tests were compared with Kruskall-Wallis tests ($p \leq .05$) and effect sizes were calculated (eta-squared).

A detailed exploration of “posterior” brain functions, through a battery specifically conceived for PCA patients which was previously described (Migliaccio et al., 2016), was also administered. This battery

was designed to investigate more “dorsal” deficits such as elements of Balint's and Gerstmann's syndromes, motor apraxia, ideomotor apraxia and visual neglect, as well as more “ventral” deficits such as alexia and visual agnosia. Patients were classified as impaired or not impaired on these symptoms and rates of subjects impaired in each group (PCA-tAD, PCA-aAD and PCA-nonAD) were compared with Fisher's exact test of independence ($p \leq .05$) and effect sizes were calculated (Cramer's V).

2.3. Magnetic resonance imaging (MRI)

2.3.1. MRI acquisition

PCA patients, as well as a group of 30 age- and gender-matched healthy subjects (CTRL, men/women: 14/16; mean age = 61.5; standard deviation = 8.4; age range = 45–79), underwent the MRI protocol. Brain MRI were acquired with a 3 T system (Siemens, Erlangen, Germany) at the Center for Magnetic Resonance Research (CENIR), Brain and Spine Institute (ICM), Paris. A high-resolution structural volume was acquired using a T1-weighted 3D magnetization prepared rapid gradient echo (MPRAGE) sequence (160 sagittal images; thickness 1 mm; FOV 256 × 256 mm^2; matrix size 256 × 256). Eight PCA patients (two PCA-tAD, four PCA-aAD and two PCA-nonAD) were scanned with compatible parameters but on a different MRI machine. The type of MRI machine was therefore added as a control covariate in our statistical analyses.

2.3.2. MRI pre-processing

Structural images were preprocessed using voxel-based morphometry (VBM) implemented in SPM12 using MATLAB 7.14.0.739 (Mathworks, Natick, MA). The images were segmented into GM and white matter. Affine registered tissue segments were used to create a custom template using the DARTEL (diffeomorphic anatomical registration using exponentiated lie algebra) approach (Ashburner, 2007). For each participant, the flow fields were calculated during a template creation, which described the transformation from each native GM image to the template. These were then applied to each participant's GM image. The VBM analysis was based on modulated GM images, where the GM value for each voxel was multiplied by the Jacobian determinant derived from spatial normalization to preserve the total amount of GM from the original images (Ashburner and Friston, 2000). The resulting modulated and normalized images were then smoothed with a Gaussian kernel of 8 mm FWHM.

2.3.3. VBM analyses

The VBM analyses were performed on smoothed GM images. First, GM maps were compared between all PCA patients and controls using an ANOVA model adjusting for subject's age, gender, MRI machine and total intracranial volume.

Groups were entered separately in the statistical model in the following order: CTRL, PCA-tAD, PCA-aAD and PCA-nonAD. The following sets of linear contrasts were set in order to identify differences in GM volume in: 1) each PCA group *vs.* healthy subjects (PCA-tAD *vs.* CTRL: [1 -1 0 0]; PCA-aAD *vs.* CTRL: [1 0 -1 0]; PCA-nonAD *vs.* CTRL: [1 0 0 -1]); 2) all PCA groups combined *vs.* healthy subjects [3 -1 -1 -1]; 3) each PCA group *vs.* the other two PCA groups (PCA-tAD *vs.* PCA-aAD and PCA-nonAD [0 -2 1 1]; PCA-aAD *vs.* PCA-tAD and PCA-nonAD [0 1 -2 1]; PCA-nonAD *vs.* PCA-tAD and PCA-aAD [0 1 1 -2];).

A first analysis was performed with the aim of investigating regions of common atrophy across PCA groups in comparison to CTRL (the results of contrast 2 were inclusively masked by all contrasts of set 1). This inclusive masking procedure limits the main effect contrast to

Table 1
Demographic, biological, clinical and cognitive characteristics of PCA-tAD, PCA-aAD and PCA-nonAD patients at the time of imaging acquisition.

	PCA-tAD (n = 13)	PCA-aAD (n = 9)	PCA-nonAD (n = 5)	Difference	Effect size
Demographics					
Age (mean ± SD)	62.6 (5.5)	63.9 (3.2)	66.5 (5.5)	$p = .491$	
Age range	53–69	60–70	61–76		
Gender (M/F)	4/9	5/4	3/2	$p = .399$	
Disease duration (years; mean ± SD)	3.6 (2.3)	4.8 (1.9)	4.1 (1.2)	$p = .194$	.009[a]
MMSE (mean ± SD)	19.2 (5.0)	21.4 (3.2)	20.6 (7.9)	$p = .530$	**.03**[a]
$A\beta_{1–42}$ (pg/ml)	310.9 (80.9)	302.9 (114.5)	726.2 (321.7)	$p = .003$	
P-Tau (pg/ml)	92.5 (33.2)	50.0 (9.3)	50.6 (10.4)	$p = .000$	
T-Tau (pg/ml)	692.2 (301.4)	305.8 (67.3)	312.2 (54.9)	p = .000	
Frontal symptoms (mean ± SD)					
Frontal assessment battery (FAB)	11.4 (3.6)	12.3 (2.6)	9.2 (5.1)	$p = .380$	.003[a]
Verbal span backwards	3.1 (1.2)	2.9 (0.9)	2.8 (0.8)	$p = .611$	**.04**[a]
Spatial span backwards	1.5 (1.1)	2.0 (1.3)	1.4 (2.2)	$p = .474$	**.02**[a]
Phonemic fluency	14.1 (8.2)	17.8 (7.4)	15.6 (8.2)	$p = .567$	**.04**[a]
Category fluency	11.0 (5.8)	16.2 (4.1)	15.4 (8.8)	$p = .083$	**.12**[a]
Parietal/dorsal symptoms (% of impaired patients)					
Balint syndrome					
Ocular apraxia	27%	63%	40%	$p = .317$	**.31**[b]
Optic ataxia	54%	75%	60%	$p = .770$	**.19**[b]
Simultagnosia	85%	100%	80%	$p = .560$	**.25**[b]
Gerstmann syndrome					
Acalculia	69%	78%	60%	$p = .865$	**.14**[b]
Agraphia	77%	56%	60%	$p = .562$	**.21**[b]
Finger agnosia	54%	33%	60%	$p = .596$	**.21**[b]
Right-left disorientation	39%	44%	40%	$p = 1.000$	.06[b]
Motor apraxia	58%	56%	80%	$p = .757$	**.19**[b]
Ideomotor apraxia	70%	89%	80%	$p = .715$	**.21**[b]
Visual neglect	85%	100%	75%	$p = .390$	**.27**[b]
Occipito-temporal/ventral symptoms (% of impaired patients)					
Alexia	69%	100%	80%	$p = .179$	**.34**[b]
Visual agnosia	77%	75%	80%	p = 1.000	.04[b]

Meaningful values are in bold.
[a] Eta squared (η^2) [in which .02 = small effect; .13 = medium effect; .26 = large effect (Cohen, 1988)].
[b] Cramer's V [in which .1 = small effect; .3 = medium effect; .5 = large effect (Cohen, 1988)].

regions that are present in each PCA group vs. CTRL contrast. A second analysis was performed in order to identify GM atrophy in each PCA group vs. CTRL (contrast set 1). A third analysis was performed with the aim of investigating regions of atrophy in comparison to CTRL that are specific to each PCA group (the relevant contrast from contrast 1 (e.g., PCA-tAD vs. CTRL) were inclusively masked by the appropriate contrast from set 3 (e.g., PCA-tAD vs. PCA-atAD and PCA-nonAD). A significance threshold of $p \leq .05$ corrected for multiple comparisons (family-wise error) was used for the second analysis and of $p \leq .001$ uncorrected for the first and third analyses. To decrease the risk of false positive results, clusters of < 20 voxels were not considered.

2.4. Positron emission tomography (PET)

2.4.1. PET acquisition

A subset of eight PCA patients (five PCA-tAD and three PCA-nonAD) as a well as a group of 17 age- and gender-matched healthy subjects (CTRL) underwent the PET protocol (Male/Female: 8/9; mean age = 63.2; standard deviation = 6.6; age range = 54–76). Brain ^{18}F-FDG PET scans were acquired 30 minutes after injection of 2 MBq/kg of 2-deoxy-2-(^{18}F)fluoro-D-glucose. All acquisitions were performed in a single session on a Philips Gemini GXL scanner and consisted of 3×5 min' frames with a voxel size of $2 \times 2 \times 2\,mm^3$. Images were then reconstructed using iterative LOR-RAMLA algorithm. Lastly, frames were realigned, summed and quality-checked.

2.4.2. PET pre-processing

All images were normalized to MNI space with a standard ^{18}F-FDG PET template using SPM8 (http://www.fil.ion.ucl.ac.uk/spm/software/spm8/) and smoothed with a Gaussian kernel of 12 mm FWHM. Parametric PET images were then created for each subject, by dividing each voxel with the mean activity extracted from a reference region. For this study, we used the pons region available on the pickatlas toolbox (http://www.nitrc.org/projects/wfu_pickatlas/).

2.4.3. PET analyses

The contrasts used for the VBM analyses were replicated with the same parameters for the PET analyses (Section 2.3.3).

3. Results

3.1. Demographic and CSF data

Out of the 27 PCA patients in this study, 13 patients were classified as PCA-tAD (48%), nine as PCA-aAD (33%) and five patients as PCA-nonAD (19%). Demographics and CSF data of patients are presented in Table 1. No differences were found in terms of age, disease duration and global cognition (as assessed with MMSE) between patients' groups.

3.2. Clinical and cognitive data

Clinical and cognitive characteristics of PCA-tAD, PCA-aAD and PCA-nonAD patients are presented in Table 1. No significant difference was observed between groups of patients. However, meaningful effect sizes were found for several measures including the MMSE (Table 1), which suggests a tendency towards statistical significance. Overall, PCA patients presented mild-to-moderate global cognitive impairment as well as typical dorsal and ventral symptoms that are characteristic of PCA. Both verbal and visuospatial working memory was impaired, while phonemic and categorical verbal fluency remained in the normal range.

Table 2
A) Brain regions included in the common pattern of GM atrophy across PCA groups *vs*. CTRL ($p \leq .05$ FWE corrected; CTRL n = 30; PCA-tAD n = 13; PCA-aAD n = 9; PCA-nonAD n = 5). B) Brain regions included in the common pattern of hypometabolism across PCA groups *vs*. CTRL ($p \leq .05$ FWE corrected; CTRL n = 17; PCA-tAD $n = 5$; PCA-nonAD $n = 3$).

Anatomical region	Side	MNI coordinates			T value	p (corr.)
		x	y	z		
A) Gray matter atrophy						
Occipital lobe						
Lingual gyrus	R	20	−93	−9	8.12	.000
	L	−26	−90	−14	8.59	.000
Middle occipital gyrus	L	−32	−80	33	8.57	.000
	L	−35	−86	9	8.98	.000
Parietal lobe						
Angular gyrus	R	39	−71	39	7.61	.000
	L	−39	−62	47	5.93	.002
Inferior parietal lobule	R	51	−42	47	7.26	.000
	L	−48	−44	44	6.38	.000
Middle cingulate cortex	R	2	−35	38	8.50	.000
	L	−3	−8	50	4.85	.040
Precuneus	R	8	−63	35	7.92	.000
	L	−6	−69	32	8.16	.000
Supramarginal gyrus	R	59	−44	35	7.48	.000
	L	−59	−39	33	5.66	.004
Temporal lobe						
Fusiform gyrus	R	32	−63	−12	9.68	.000
	L	−33	−60	−12	8.49	.000
Inferior temporal gyrus	R	63	−47	−14	9.04	.000
	L	−51	−62	−5	8.92	.000
Middle temporal gyrus	R	65	−33	−3	8.41	.000
	R	50	−68	11	9.23	.000
	L	−62	−50	6	5.95	.001
Frontal lobe						
Inferior frontal gyrus (pars opercularis)	R	45	15	32	6.37	.000
Middle frontal gyrus	L	−23	26	45	6.09	.000
Postcentral gyrus	R	59	−17	33	5.49	.006
Precentral gyrus	R	30	−6	57	6.37	.000
	L	−42	9	35	5.57	.005
Superior frontal gyrus	R	23	38	36	5.49	.006
	L	−24	−6	57	6.43	.000
Thalamus	R	3	−12	5	5.86	.002
Cerebellum						
Cerebellum (VIII)	R	36	−50	−44	5.58	.005
	L	−36	−59	−54	5.56	.005
B) Hypometabolism						
Occipital lobe						
Middle occipital gyrus	R	44	−76	2	10.53	.000
	L	−34	−76	28	7.84	.005
Calcarine gyrus	R	4	−88	−10	7.36	.011
Inferior occipital gyrus	R	38	−86	−16	6.70	.031
	L	−50	−74	−4	8.88	.001
Middle occipital gyrus	L	−38	−70	8	8.23	.003
Superior occipital gyrus	L	−28	−94	24	8.00	.004
	L	−18	−76	40	8.59	.002
Parietal lobe						
Angular gyrus	R	46	−78	38	6.78	.027
	R	40	−64	34	7.99	.004
Inferior parietal lobule	L	−34	−54	40	8.45	.002
Precuneus	R	14	−60	36	6.80	.026
Superior parietal lobule	R	22	−76	52	7.88	.005
	L	−16	−72	54	9.42	.000
Temporal lobe						
Inferior temporal gyrus	R	52	−64	−16	9.00	.001
	L	−48	−56	−14	11.15	.000
	L	−48	−38	−16	9.50	.000

Abbreviations: R = Right; L = Left.

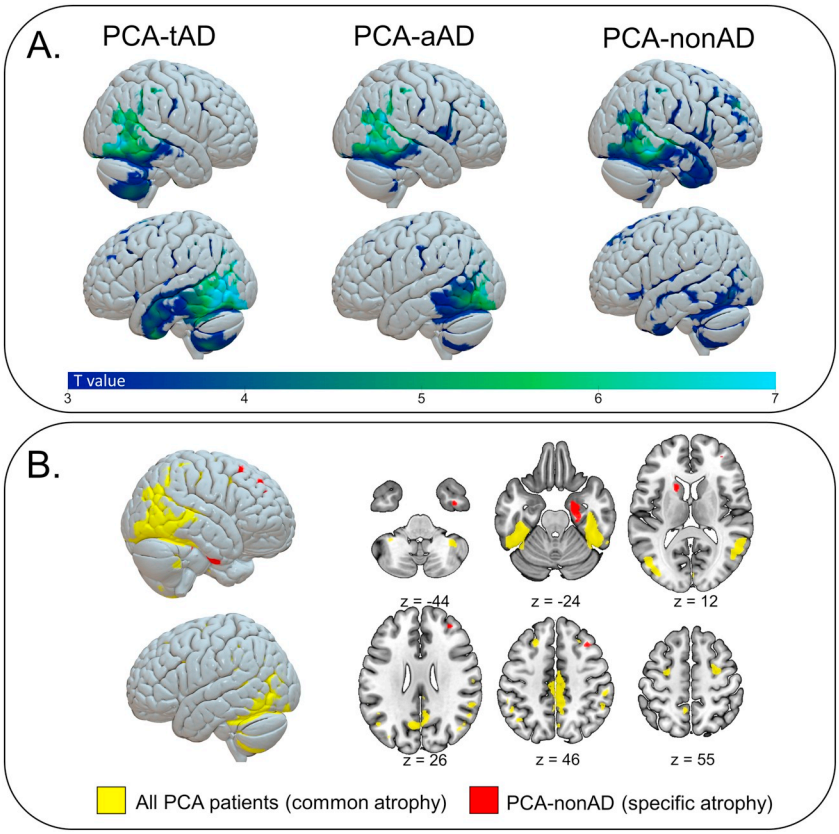

Fig. 1. GM atrophy. A) Atrophy in each PCA group vs. CTRL ($p \leq .001$ uncorrected; CTRL $n = 30$; PCA-tAD $n = 13$; PCA-aAD $n = 9$; PCA-nonAD $n = 5$). B) Brain regions included in the common pattern of GM atrophy across PCA groups *vs.* CTRL (yellow; $p \leq .05$ FWE corrected) and PCA-nonAD group-specific atrophy (red; $p \leq .001$ but also significant at $p \leq .05$ FWE corrected). Color bar represents T values.

3.3. GM atrophy and hypometabolism

3.3.1. Common pattern of GM atrophy and hypometabolism across PCA groups vs CTRL

Brain regions included in the common pattern of GM atrophy across PCA groups ($n = 27$) in comparison to CTRL ($n = 30$) are presented in Table 2 and Fig. 1A. All PCA patients shared a large region of brain damage mainly including bilateral associative parieto-occipital, precuneus, posterior cingulate, posterior temporal regions, as well as frontal and cerebellum regions ($p \leq .05$ FWE corrected).

Brain regions included in the common pattern of hypometabolism across PCA ($n = 8$) groups in comparison to CTRL ($n = 17$) are presented in Table 2 and Fig. 2A. Shared hypometabolism in all PCA patients extended a bit more posteriorly and included bilateral associative parieto-occipital, precuneus and posterior temporal regions ($p \leq .05$ FWE corrected).

3.3.2. GM atrophy and hypometabolism in each PCA group vs. CTRL

In terms of GM atrophy (Fig. 1A, supplementary tables 1–3), each PCA group showed bilateral parietal, occipital and posterior temporal GM atrophy. PCA-tAD's pattern of atrophy also involved left anterior temporal regions and bilateral cerebellum ($p \leq .001$ uncorrected; $n = 13$). Small areas of frontal atrophy were observed in PCA-tAD and PCA-aAD ($n = 9$) groups. However, the PCA-nonAD group ($n = 5$) presented with more diffuse frontal and temporal atrophy, especially in the right hemisphere.

Hypometabolism analyses were conducted on a subset of five PCA-tAD and three PCA-nonAD. PET imaging was not available for any of the PCA-aAD patients. Both PCA-tAD and PCA-nonAD group showed bilateral parietal, occipital and posterior temporal hypometabolism (Fig. 2A, supplementary tables 1–3; $p \leq .001$ uncorrected). In PCA-tAD, hypometabolism extended anteriorly in the temporal lobes and in the cerebellum. In PCA-nonAD, hypometabolism extended to the frontal regions.

3.3.3. Specific pattern of atrophy and hypometabolism to each PCA group vs. CTRL

No specific areas of GM atrophy were found for PCA-tAD patients and PCA-aAD. Conversely, PCA-nonAD patients presented a group-specific pattern of atrophy including the left caudate nucleus, right dorsolateral prefrontal cortex and middle frontal gyrus, as well as the right anterior medial temporal regions in comparison to CTRL ($p \leq .001$ uncorrected but also significant at $p \leq .05$ FWE corrected; Table 3 and Fig. 1B).

In terms of hypometabolism, the analyses on a subset of patients showed that PCA-tAD patients presented a specific pattern of hypometabolism in the left inferior temporal gyrus ($x = -44$, $y = -14$; $z = -36$; $t = 8.28$; $p \leq .001$ uncorrected but also significant at $p \leq .05$ FWE corrected; Fig. 2B). PCA-nonAD patients presented a specific pattern of hypometabolism including the right supplementary motor area and the right paracentral lobule ($p \leq .001$ uncorrected; Table 3 and Fig. 2B).

3.4. Ancillary results: nigrostriatal dopaminergic denervation

A subset of three PCA-nonAD patients underwent single-photon emission computed tomography (SPECT) dopamine transporter imaging to investigate the presence of nigrostriatal dopaminergic denervation (frequent in dementia with Lewy bodies pathology; DLB, (McCleery et al., 2015) and corticobasal degeneration pathology; CBD) (Mille et al., 2016). Briefly, patients received potassium iodide to block thyroid uptake before tracer injection. Brain perfusion scintigraphy was acquired three hours after the intravenous injection of 185 MBq of 123I-FP-CIT (DaTSCAN; GE Healthcare) with a three-headed gamma camera equipped with parallel high-resolution collimators (Irix; Philips, Eindhoven, The Netherlands). All three patients presented nigrostriatal dopaminergic denervation.

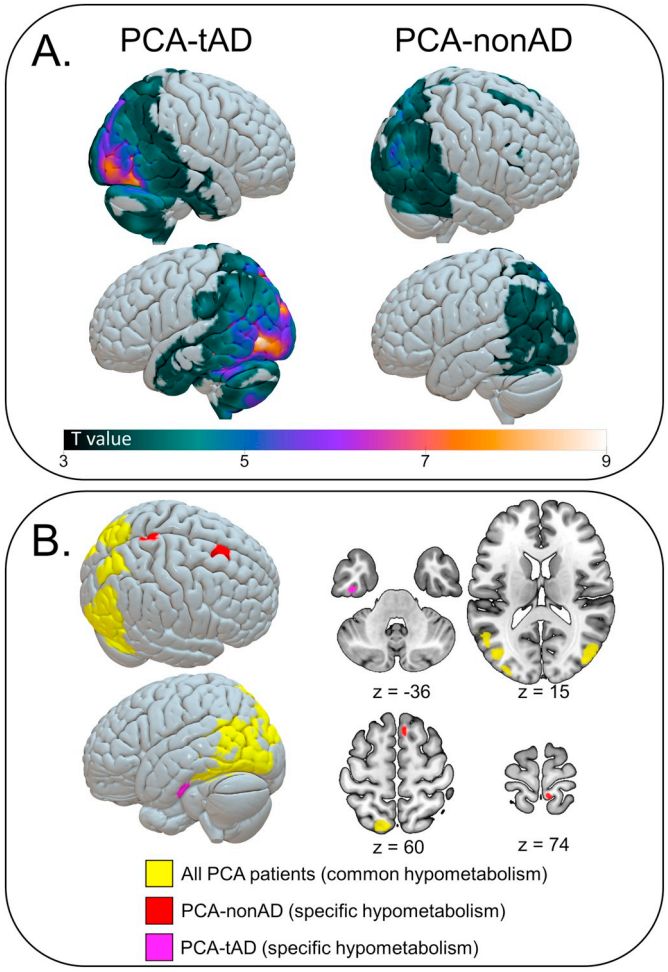

Fig. 2. Hypometabolism. A) Hypometabolism in PCA-tAD vs. CTRL and PCA-nonAD vs. CTRL ($p \leq .001$ uncorrected; CTRL $n = 17$; PCA-tAD n = 5; PCA-nonAD n = 3). B) Brain regions included in the common pattern of hypometabolism across PCA groups *vs.* CTRL (yellow; $p \leq .05$ FWE corrected), PCA-nonAD group-specific hypometabolism (red; $p \leq .001$ uncorrected) and PCA-aAD group-specific hypometabolism (pink; $p \leq .001$ uncorrected but also significant at $p \leq .05$ FWE corrected). Color bar represents T values.

4. Discussion

The present study reports, for the first time, a detailed exploration of a large group of patients on the PCA spectrum. We compared brain atrophy, brain hypometabolism and clinical/cognitive profiles in PCA patients according to their AD CSF biomarkers profiles.

As expected, we found that PCA was most frequently associated with AD pathology (81%), in agreement with previous *in vivo* (Beaufils et al., 2013; Beaufils et al., 2014; Coppi et al., 2014; de Souza et al., 2011a; de Souza et al., 2011b; Seguin et al., 2011) and *post-mortem* (Renner et al., 2004; Tang-Wai et al., 2004) studies. More precisely, 48% presented the typical AD CSF profile (PCA-tAD; abnormal $A\beta_{1-42}$ and T-tau/P-Tau biomarkers), and 33% presented the atypical AD CSF profile (PCA-aAD; isolated $A\beta_{1-42}$ decrease). The isolated $A\beta_{1-42}$ decrease is thought to be consistent with AD pathology, although it might be less specific than the typical AD CSF profile (Beaufils et al., 2013; Beaufils et al., 2014; Coppi et al., 2014; Seguin et al., 2011). According to the A/T/N model (Jack Jr. et al., 2018; Jack Jr. et al., 2016), both A + T+ N+ (PCA-tAD) and A + T-N- (PCA-aAD) patients are on the AD continuum, but are differentially labelled as "Alzheimer's disease" and "Alzheimer's pathologic change". Within this framework, the $A\beta_{1-42}$ decrease means an early upstream pathophysiological process, whereas CSF T-tau level, for example, can be considered as a biomarker of downstream pathophysiological processes (Jack et al., 2011).

Nineteen percent presented a non-AD CSF profile, indicating that AD is not the underlying pathological substrate in these PCA cases. However, this CSF profile does not allow for the precise identification of the pathology. Non-AD pathologies such as CBD, DLB, and Creutzfeldt-Jakob disease have been described as possible in PCA (Renner et al., 2004; Tang-Wai et al., 2004). Creutzfeldt-Jakob disease is associated with a very rapid disease progression and can therefore be ruled out in the presented PCA-nonAD cases, leaving CBD and DLB as the most plausible causes. In our study, we did not detect extrapyramidal symptoms, cognitive fluctuations or visual hallucinations in PCA-nonAD patients at symptom onset or at the time of neuroimaging acquisition. However, all patients from that group who afterwards underwent SPECT dopamine transporter imaging presented a nigrostriatal dopaminergic denervation. These findings provide support to underlying CBD or DLB (McCleery et al., 2015; Mille et al., 2016) in these patients, which can both present without clear and early motor manifestations (Bonner et al., 2003; Lee et al., 2011; Sakurai and Nakashima, 2017). In these cases, a longitudinal follow-up is essential to assess if over time, they will develop CBD or DLB features. Interestingly, out of five PCA-nonAD patients, only two of them had developed such features two to three years after their inclusion in the present study. One patient had developed clear visual hallucinations at their 3-year follow-up, which might be consistent with DLB pathology. Another patient had developed a discrete asymmetric akinetic-rigid syndrome and an accentuation of frontal symptoms at their 2-year follow-up, which might be consistent with CBD pathology.

In terms of brain damage, all PCA patients, independently of biological substrate, presented a large and posterior area of brain damage encompassing occipital, parietal and posterior temporal regions. Brain damage in PCA patients with AD pathology (PCA-tAD and PCA-aAD) remained largely equivalent to this damage pattern common to all PCA patients and previously documented in the literature (Kas et al., 2011; Migliaccio et al., 2016; Whitwell et al., 2007). In contrast, when we investigated the specificities of each subgroup, PCA-nonAD patients presented specific atrophy in the left caudate nucleus, right dorsolateral prefrontal cortex and anterior medial temporal regions, and group-specific hypometabolism in the right supplementary motor area and paracentral lobule. These areas are not typically reported in PCA (Kas et al., 2011; Migliaccio et al., 2016; Whitwell et al., 2007). This might

Table 3
A) Brain regions included in the specific pattern of GM atrophy of the PCA-nonAD group *vs.* CTRL ($p \leq .001$ uncorrected; CTRL n = 30; PCA-nonAD n = 5). B) Brain regions included in the specific pattern of hypometabolism of the PCA-nonAD group *vs.* CTRL ($p \leq .001$ uncorrected; CTRL n = 17; PCA-nonAD n = 3).

Anatomical region	Side	MNI coordinates			T value	P (uncorr.)
		x	y	z		
A) Gray matter atrophy						
Frontal lobe						
Caudate nucleus	L	−17	11	15	4.97	.000*
Dorsolateral prefrontal cortex	R	32	42	32	5.36	.000*
Middle frontal gyrus	R	36	27	44	4.79	.000*
Temporal lobe						
Parahippocampal gyrus	R	23	−20	−24	5.66	.000*
Inferior temporal gyrus	R	39	−5	−44	5.26	.000*
B) Hypometabolism						
Frontal lobe						
Supplementary motor area	R	8	20	60	4.58	.000
Parietal lobe						
Paracentral lobule	R	8	−42	78	5.24	.000

Abbreviations: R = Right; L = Left.
* Also significant at $p \leq .05$ FWE corrected.

be due to the fact that PCA-nonAD patients are rare (Seguin et al., 2011). Given that rarity, no previous study has investigated differences between PCA subgroups based on biological characterization, but they are rather included in general PCA groups for analyses. Interestingly, the regions in which grey matter and metabolism changes have been observed in PCA-nonAD patients highly overlap with regions affected in CBD and DLB, with a strong hemispheric lateralization (Lee et al., 2011; Su et al., 2015; Whitwell et al., 2017; Zhong et al., 2014). This provides additional support for underlying CBD and DLB pathology in our PCA-nonAD patients. Indeed, independently of the clinical presentation, the core regions affected in patients with CBD are the dorsal prefrontal cortex, the supplementary motor area, the perirolandic cortex and the striatum (Lee et al., 2011) with an asymmetry often reported between the hemispheres. In DLB patients, atrophy and hypometabolism in frontal, caudate nucleus and anterior temporal regions was previously described in comparison to both normal subjects (Su et al., 2015; Zhong et al., 2014) and patients affected by typical PCA syndrome (Whitwell et al., 2017). Underlying CBD or DLB pathology in our PCA-nonAD cases is a potential cause of the group-specific frontal and mesio-temporal damage observed in this group in the present study. Finally, PCA-tAD also showed group-specific hypometabolism in the left inferior temporal gyrus, corresponding to the more extensive temporal atrophy which is highly visible in this group (i.e. in the direct contrast between PCA-tAD and CTRL). This region is part of the so-called visual ventral stream which is typically impaired in PCA patients with AD pathology [(Migliaccio et al., 2012b), also see occipito-temporal PCA in (Alladi et al., 2007)]. This result is also consistent with previous imaging studies in PCA-AD patients showing decreased functional connectivity in the ventral stream (Migliaccio et al., 2016). More generally, it seems to suggest a more widespread neurodegeneration in this PCA subtype.

The multimodal nature of our study highlights the importance of neuroimaging in both the diagnosis and characterization of PCA. In the present study, both MRI and PET results show a consistent epicenter of brain damage in PCA patients in bilateral parietal, occipital and posterior temporal regions. Nonetheless, our PET results revealed a more extended hypometabolism in associative regions in comparison to the GM atrophy pattern showed by our MRI results, although the PET analyses included a lower sample size. This could suggest that PET is a more sensitive neuroimaging tool in comparison to MRI in the detection of brain damage in PCA patients. This is in accordance with the French guidelines, which recommend the use of PET in addition to morphological MRI to detect characteristic metabolism changes in posterior associative cortices in atypical presentations of AD (Haute Autorité de Santé (HAS), 2011). The clinical utility of PET was also highlighted in a previous meta-analysis in which it achieved the highest area under the receiver operating curve (0.96) for the diagnosis of AD, in comparison to CSF biomarkers and MRI GM atrophy, with a sensitivity of 90% and a specificity of 89% (Bloudek et al., 2011). Furthermore, the present multimodal approach was able to detect subtle anatomo-functional differences among patients presenting with the same cognitive profile, namely the temporal involvement in PCA-tAD and the frontal involvement in PCA-nonAD.

In terms of clinical profiles, all three PCA groups presented with typical visual and visuospatial impairments, irrespectively of their biological substrate (tAD, aAD or non-AD) and consistently with the common pattern of brain damage. No statistical difference was observed between the groups on any of the demographic or clinical/cognitive variables. This might be due to the low sample size in some of our groups, which is supported by the fact that meaningful effect sizes were found for several measures. With careful investigation, two statistical trends emerged: the more frequent presence of motor apraxia in PCA-nonAD patients, suggesting a probable CBD pathology, and a trend towards less severe cognitive symptoms (i.e. MMSE global score) in the PCA-aAD group, at a comparable level of brain damage. These observations suggest that an extensive and careful assessment of frontal and motor symptoms as well as a longitudinal follow-up of PCA patients would be essential to improve anatomo-clinical diagnosis. For example, the presence of motor apraxia in as many as 80% of PCA-nonAD patients will need clinical confirmation. Moreover, PCA patients presenting with an isolated $A\beta_{1-42}$ decrease (amyloidogenic process) and normal T-tau/P-Tau (absence of severe neuronal death) seem to show a less aggressive disease. Longitudinal studies on larger samples, including all phenotypical variants of AD (early onset, late onset, other focal variants) would be necessary to further investigate this hypothesis.

The present study has some limitations. In terms of the sample, the number of subjects was different between the MRI and PET data. While all PCA patient underwent MRI and clinical/cognitive assessment, only a subset of these patients underwent the ^{18}F-FDG PET scan. This limits the interpretation of the results between the two neuroimaging modalities. In terms of the clinical/cognitive assessment, some cognitive functions were only computed as binary variables (impaired/unimpaired), and frontal, memory, language and praxis functions were not extensively assessed, which could partially explain the lack of significant difference in the cognitive/clinical profiles across the PCA spectrum. In particular, memory and language were assessed for diagnosis purposes, but the data was not usable for research purposes (heterogeneity in assessment tools used, assessment conducted at different time points than the MRI, etc.). Finally, while our study is the first to investigate *in vivo* differences between PCA patients across the AD pathology spectrum, none of our subjects had *post-mortem* pathological diagnosis confirmation.

This study adds new insights to the limited literature investigating *in vivo* differences between PCA with diverse neuropathological substrates. On one hand, we can conclude that irrespectively of the underlying biological disease, the posterior brain regions are invariably impaired across the PCA spectrum. On the other hand, the underlying pathologies have an impact at least on the anatomical and metabolic brain patterns, because PCA-nonAD presented with an additional fronto-temporal (especially dorsolateral frontal) damage. The identification of three CSF profiles also should be taken in account: with the growing development of protein-specific therapies for AD, a better understanding of the impact of different underlying pathologies and profiles on the clinico-anatomical presentation is necessary. These results warrant the need for longitudinal follow-ups to investigate the clinical and anatomical evolution of PCA with atypical CSF AD profile, and the occurrence of frontal symptoms in PCA. Typical posterior symptoms represent the clinical hallmark of the disease, no matter the underlying pathology, but frontal and motor symptoms might become more important with the evolution of the disease, specifically in PCA-nonAD. Future studies should also study PCA patients using network-based or structural connectivity neuroimaging approaches, as their ability to discriminate other neurologic samples according to their underlying pathologies (Mahoney et al., 2014; Medaglia et al., 2017).

Acknowledgements

The study is supported by “France Alzheimer” and “Philippe Chatrier” foundations. M. Montembeault acknowledges the support of Quebec Bio Imaging Network and Fonds de recherche du Québec en Santé.

M. Montembeault, S.M. Brambati, F. Lamari, A. Michon, D. Samri, L. Lacomblez, S. Lehéricy & R. Migliaccio report no conflicts of interest. B. Dubois has received consulting fees from Eli Lilly. S. Epelbaum has received speaker honoraria from GE Healthcare, BIOGEN and Astellas Pharma. M.O. Habert has received speaker honoraria from Lilly, GE Healthcare and Piramal. A. Kas has received speaker honoraria from GE Healthcare and Piramal.

Appendix A. Supplementary data

Supplementary data to this article can be found online at https://

doi.org/10.1016/j.nicl.2018.10.010.

References

Alladi, S., Xuereb, J., Bak, T., Nestor, P., Knibb, J., Patterson, K., Hodges, J.R., 2007. Focal cortical presentations of Alzheimer's disease. Brain 130, 2636–2645.

Ashburner, J., 2007. A fast diffeomorphic image registration algorithm. NeuroImage 38, 95–113.

Ashburner, J., Friston, K.J., 2000. Voxel-based morphometry—the methods. NeuroImage 11, 805–821.

Baldacci, F., Toschi, N., Lista, S., Zetterberg, H., Blennow, K., Kilimann, I., Teipel, S., Cavedo, E., dos Santos, A.M., Epelbaum, S., Lamari, F., Dubois, B., Floris, R., Garaci, F., Bonuccelli, U., Hampel, H., 2017. Two-level diagnostic classification using cerebrospinal fluid YKL-40 in Alzheimer's disease. Alzheimers Dement. 13, 993–1003.

Beaufils, E., Dufour-Rainfray, D., Hommet, C., Brault, F., Cottier, J.P., Ribeiro, M.J., Mondon, K., Guilloteau, D., 2013. Confirmation of the amyloidogenic process in posterior cortical atrophy: value of the Abeta42/Abeta40 ratio. J. Alzheimers Dis. 33, 775–780.

Beaufils, E., Ribeiro, M.J., Vierron, E., Vercouillie, J., Dufour-Rainfray, D., Cottier, J.P., Camus, V., Mondon, K., Guilloteau, D., Hommet, C., 2014. The pattern of brain amyloid load in posterior cortical atrophy using (18)F-AV45: is amyloid the principal actor in the disease? Dement. Geriatr. Cogn. Dis. Extra 4, 431–441.

Benson, D.F., Davis, R.J., Snyder, B.D., 1988. Posterior cortical atrophy. Arch. Neurol. 45, 789–793.

Bloudek, L.M., Spackman, D.E., Blankenburg, M., Sullivan, S.D., 2011. Review and meta-analysis of biomarkers and diagnostic imaging in Alzheimer's disease. J. Alzheimers Dis. 26, 627–645.

Bonner, L.T., Tsuang, D.W., Cherrier, M.M., Eugenio, C.J., Du, J.Q., Steinbart, E.J., Limprasert, P., La Spada, A.R., Seltzer, B., Bird, T.D., Leverenz, J.B., 2003. Familial dementia with lewy bodies with an atypical clinical presentation. J. Geriatr. Psychiatry Neurol. 16, 59–64.

Cohen, J., 1988. Statistical Power Analysis for the Behavioral Sciences. Routledge.

Coppi, E., Ferrari, L., Santangelo, R., Caso, F., Pinto, P., Passerini, G., Comi, G., Magnani, G., 2014. Further evidence about the crucial role of CSF biomarkers in diagnosis of posterior cortical atrophy. Neurol. Sci. 35, 785–787.

Dubois, B., Slachevsky, A., Litvan, I., Pillon, B., 2000. The FAB: a Frontal Assessment Battery at bedside. Neurology 55, 1621–1626.

Dubois, B., Feldman, H.H., Jacova, C., Hampel, H., Molinuevo, J.L., Blennow, K., DeKosky, S.T., Gauthier, S., Selkoe, D., Bateman, R., Cappa, S., Crutch, S., Engelborghs, S., Frisoni, G.B., Fox, N.C., Galasko, D., Habert, M.O., Jicha, G.A., Nordberg, A., Pasquier, F., Rabinovici, G., Robert, P., Rowe, C., Salloway, S., Sarazin, M., Epelbaum, S., de Souza, L.C., Vellas, B., Visser, P.J., Schneider, L., Stern, Y., Scheltens, P., Cummings, J.L., 2014. Advancing research diagnostic criteria for Alzheimer's disease: the IWG-2 criteria. Lancet Neurol. 13, 614–629.

Folstein, M.F., Folstein, S.E., McHugh, P.R., 1975. "Mini-mental state". A practical method for grading the cognitive state of patients for the clinician. J. Psychiatr. Res. 12, 189–198.

Jack Jr., C.R., Bennett, D.A., Blennow, K., Carrillo, M.C., Feldman, H.H., Frisoni, G.B., Hampel, H., Jagust, W.J., Johnson, K.A., Knopman, D.S., Petersen, R.C., Scheltens, P., Sperling, R.A., Dubois, B., 2016. A/T/N: An unbiased descriptive classification scheme for Alzheimer disease biomarkers. Neurology 87, 539–547.

Jack Jr., C.R., Bennett, D.A., Blennow, K., Carrillo, M.C., Dunn, B., Haeberlein, S.B., Holtzman, D.M., Jagust, W., Jessen, F., Karlawish, J., Liu, E., Molinuevo, J.L., Montine, T., Phelps, C., Rankin, K.P., Rowe, C.C., Scheltens, P., Siemers, E., Snyder, H.M., Sperling, R., 2018. NIA-AA Research Framework: Toward a biological definition of Alzheimer's disease. Alzheimers Dement. 14, 535–562.

Jack, C.R., Vemuri, P., Wiste, H.J., Weigand, S.D., Aisen, P.S., Trojanowski, J.Q., Shaw, L.M., Bernstein, M.A., Petersen, R.C., Weiner, M.W., Knopman, D.S., 2011. Evidence for Ordering of Alzheimer's Disease Biomarkers. Arch. Neurol. 68, 1526–1535.

Kas, A., de Souza, L.C., Samri, D., Bartolomeo, P., Lacomblez, L., Kalafat, M., Migliaccio, R., Thiebaut de Schotten, M., Cohen, L., Dubois, B., Habert, M.O., Sarazin, M., 2011. Neural correlates of cognitive impairment in posterior cortical atrophy. Brain 134, 1464–1478.

Kremin, H., Perrier, D., de Wilde, M., 1999. DENO 100- Paradigme expérimental et test clinique de dénomination contrôlée : effet relatif de 7 variables expérimentales sur les performances de 16 sujets atteints de maladies dégénératives. Rev. Neuropsychol. 9, 439–440.

Lee, S.E., Rabinovici, G.D., Mayo, M.C., Wilson, S.M., Seeley, W.W., DeArmond, S.J., Huang, E.J., Trojanowski, J.Q., Growdon, M.E., Jang, J.Y., Sidhu, M., See, T.M., Karydas, A.M., Gorno-Tempini, M.L., Boxer, A.L., Weiner, M.W., Geschwind, M.D., Rankin, K.P., Miller, B.L., 2011. Clinicopathological correlations in corticobasal degeneration. Ann. Neurol. 70, 327–340.

Mahoney, C.J., Ridgway, G.R., Malone, I.B., Downey, L.E., Beck, J., Kinnunen, K.M., Schmitz, N., Golden, H.L., Rohrer, J.D., Schott, J.M., Rossor, M.N., Ourselin, S., Mead, S., Fox, N.C., Warren, J.D., 2014. Profiles of white matter tract pathology in frontotemporal dementia. Hum. Brain Mapp. 35, 4163–4179.

McCleery, J., Morgan, S., Bradley, K.M., Noel-Storr, A.H., Ansorge, O., Hyde, C., 2015. Dopamine transporter imaging for the diagnosis of dementia with Lewy bodies. Cochrane Database of Systematic Reviews. https://doi.org/10.1002/14651858.CD010633.pub2. (Issue 1. Art. No.: CD010633).

McKhann, G.M., Knopman, D.S., Chertkow, H., Hyman, B.T., Jack Jr., C.R., Kawas, C.H., Klunk, W.E., Koroshetz, W.J., Manly, J.J., Mayeux, R., Mohs, R.C., Morris, J.C., Rossor, M.N., Scheltens, P., Carrillo, M.C., Thies, B., Weintraub, S., Phelps, C.H., 2011. The diagnosis of dementia due to Alzheimer's disease: recommendations from the National Institute on Aging-Alzheimer's Association workgroups on diagnostic guidelines for Alzheimer's disease. Alzheimers Dement. 7, 263–269.

McMonagle, P., Deering, F., Berliner, Y., Kertesz, A., 2006. The cognitive profile of posterior cortical atrophy. Neurology 66, 331–338.

Medaglia, J.D., Huang, W., Segarra, S., Olm, C., Gee, J., Grossman, M., Ribeiro, A., McMillan, C.T., Bassett, D.S., 2017. Brain network efficiency is influenced by the pathologic source of corticobasal syndrome. Neurology 89, 1373–1381.

Migliaccio, R., Agosta, F., Rascovsky, K., Karydas, A., Bonasera, S., Rabinovici, G.D., Miller, B.L., Gorno-Tempini, M.L., 2009. Clinical syndromes associated with posterior atrophy: early age at onset AD spectrum. Neurology 73, 1571–1578.

Migliaccio, R., Agosta, F., Possin, K.L., Rabinovici, G.D., Miller, B.L., Gorno-Tempini, M.L., 2012a. White matter atrophy in Alzheimer's disease variants. Alzheimers Dement 8 (S78–87.e71–72).

Migliaccio, R., Agosta, F., Scola, E., Magnani, G., Cappa, S.F., Pagani, E., Canu, E., Comi, G., Falini, A., Gorno-Tempini, M.L., Bartolomeo, P., Filippi, M., 2012b. Ventral and dorsal visual streams in posterior cortical atrophy: a DT MRI study. Neurobiol. Aging 33, 2572–2584.

Migliaccio, R., Gallea, C., Kas, A., Perlbarg, V., Samri, D., Trotta, L., Michon, A., Lacomblez, L., Dubois, B., Lehericy, S., Bartolomeo, P., 2016. Functional connectivity of ventral and dorsal visual streams in posterior cortical atrophy. J. Alzheimers Dis. 51, 1119–1130.

Mille, E., Levin, J., Brendel, M., Zach, C., Barthel, H., Sabri, O., Botzel, K., Bartenstein, P., Danek, A., Rominger, A., 2016. Cerebral glucose metabolism and dopaminergic function in patients with corticobasal syndrome. J. Neuroimaging 27, 255–261.

Panegyres, P.K., Goh, J., McCarthy, M., Campbell, A.I., 2017. The nature and natural history of posterior cortical atrophy syndrome: a variant of early-onset alzheimer disease. Alzheimer Dis. Assoc. Disord. 31, 295–306.

Renner, J.A., Burns, J.M., Hou, C.E., McKeel Jr., D.W., Storandt, M., Morris, J.C., 2004. Progressive posterior cortical dysfunction: a clinicopathologic series. Neurology 63, 1175–1180.

Sakurai, Y., Nakashima, Y., 2017. Progressive Balint's syndrome in a patient demonstrating dementia with lewy bodies. Intern. Med. 56, 1421–1424.

Haute Autorité de Santé (HAS), 2011. Maladie d'Alzheimer et maladies apparentées: diagnostic et prise en charge. pp. 1–48.

Seguin, J., Formaglio, M., Perret-Liaudet, A., Quadrio, I., Tholance, Y., Rouaud, O., Thomas-Anterion, C., Croisile, B., Mollion, H., Moreaud, O., Salzmann, M., Dorey, A., Bataillard, M., Coste, M.H., Vighetto, A., Krolak-Salmon, P., 2011. CSF biomarkers in posterior cortical atrophy. Neurology 76, 1782–1788.

de Souza, L.C., Corlier, F., Habert, M.O., Uspenskaya, O., Maroy, R., Lamari, F., Chupin, M., Lehericy, S., Colliot, O., Hahn-Barma, V., Samri, D., Dubois, B., Bottlaender, M., Sarazin, M., 2011a. Similar amyloid-beta burden in posterior cortical atrophy and Alzheimer's disease. Brain 134, 2036–2043.

de Souza, L.C., Lamari, F., Belliard, S., Jardel, C., Houillier, C., De Paz, R., Dubois, B., Sarazin, M., 2011b. Cerebrospinal fluid biomarkers in the differential diagnosis of Alzheimer's disease from other cortical dementias. J. Neurol. Neurosurg. Psychiatry 82, 240–246.

Su, L., Blamire, A.M., Watson, R., He, J., Aribisala, B., O'Brien, J.T., 2015. Tissue microstructural changes in dementia with Lewy bodies revealed by quantitative MRI. J. Neurol. 262, 165–172.

Tang-Wai, D.F., Graff-Radford, N.R., Boeve, B.F., Dickson, D.W., Parisi, J.E., Crook, R., Caselli, R.J., Knopman, D.S., Petersen, R.C., 2004. Clinical, genetic, and neuropathologic characteristics of posterior cortical atrophy. Neurology 63, 1168–1174.

Teichmann, M., Kas, A., Boutet, C., Ferrieux, S., Nogues, M., Samri, D., Rogan, C., Dormont, D., Dubois, B., Migliaccio, R., 2013. Deciphering logopenic primary progressive aphasia: a clinical, imaging and biomarker investigation. Brain 136, 3474–3488.

Wechsler, D., 1981. The Wechsler Adult Intelligence Scale–Revised. Psychological Corporation, San Antonio.

Whitwell, J.L., Jack Jr., C.R., Kantarci, K., Weigand, S.D., Boeve, B.F., Knopman, D.S., Drubach, D.A., Tang-Wai, D.F., Petersen, R.C., Josephs, K.A., 2007. Imaging correlates of posterior cortical atrophy. Neurobiol. Aging 28, 1051–1061.

Whitwell, J.L., Graff-Radford, J., Singh, T.D., Drubach, D.A., Senjem, M.L., Spychalla, A.J., Tosakulwong, N., Lowe, V.J., Josephs, K.A., 2017. 18F-FDG PET in posterior cortical atrophy and dementia with lewy bodies. J. Nucl. Med. 58, 632–638.

Zhong, J., Pan, P., Dai, Z., Shi, H., 2014. Voxelwise meta-analysis of gray matter abnormalities in dementia with Lewy bodies. Eur. J. Radiol. 83, 1870–1874.